HHS Public Access

Author manuscript

Free Radic Biol Med. Author manuscript; available in PMC 2023 March 01.

Published in final edited form as:

Free Radic Biol Med. 2022 March ; 182: 23–33. doi:10.1016/j.freeradbiomed.2022.02.006.

C19orf12 ablation causes ferroptosis in mitochondrial membrane protein-associated with neurodegeneration

Changjuan Shao[1], **Julia Zhu**[1,2], **Xiaopin Ma**[1], **Sandra L. Siedlak**[1], **Mark L. Cohen**[1], **Alan Lerner**[3], **Wenzhang Wang**[1]

[1]Department of Pathology, Case Western Reserve University, Cleveland, OH, USA

[2]Hathaway Brown School, Shaker Heights, OH, USA

[3]Department of Neurology, University Hospitals Case Medical Center, Beachwood, OH, USA.

Abstract

Mitochondrial membrane protein-associated with neurodegeneration (MPAN) is a rare genetic disease characterized by aggressive neurodegeneration and massive iron accumulation in patients' brains. Genetics studies identified defects in C19orf12 locus being associated with MPAN which likely caused loss of function although underlying pathogenic mechanism(s) remain elusive. In the present study, we investigated C19orf12 knockout (KO) M17 neuronal cells and primary skin fibroblasts from MPAN patients with C19orf12 homozygous G58S or heterozygous C19orf12 p99fs*102 mutations as cellular models of MPAN. C19orf12 KO cells and MPAN fibroblast cells demonstrated mitochondrial fragmentation and dysfunction, iron overload and increased oxidative damage. Antioxidant NAC and iron chelator DFO rescued both oxidative stress and mitochondrial deficits. Moreover, C19orf12 KO cells and MPAN fibroblast cells were susceptible to erastin- or RSL3-induced ferroptosis which could be almost completely prevented by pretreatment of iron chelator DFO. Importantly, we also found mitochondrial fragmentation and increased ferroptosis related oxidative damage in neurons in the biopsied cortical tissues from an MPAN patient. Collectively, these results supported the notion that iron overload and ferroptosis likely play an important role in the pathogenesis of MPAN.

Graphical Abstract

Corresponding author: Wenzhang Wang, Department of Pathology, Case Western Reserve University, 2103 Cornell Road, Cleveland, OH 44106, USA. wenzhang.wang@case.edu.

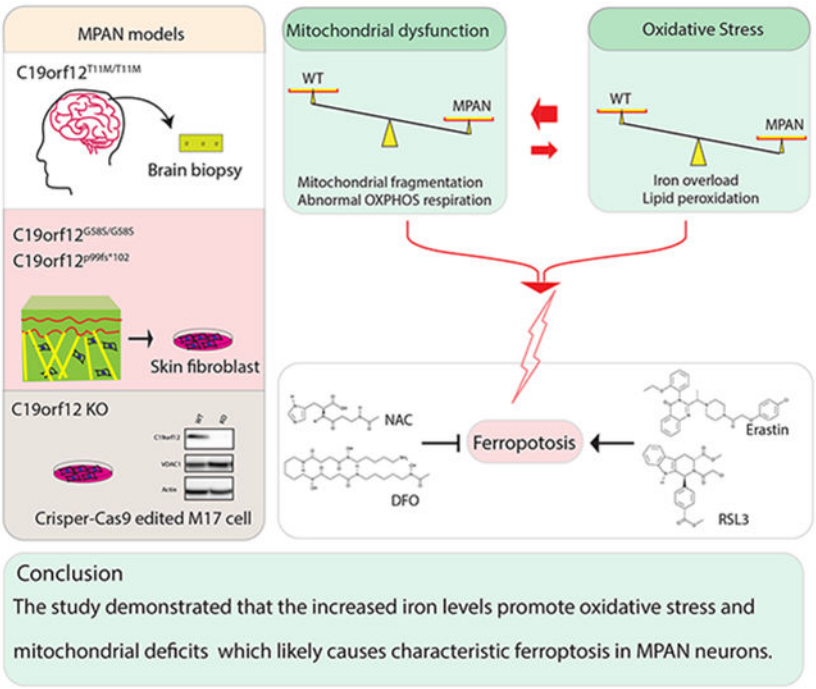

Keywords

C19orf12; mitochondrial dysfunction; oxidative stress; iron accumulation; ferroptosis; MPAN

Introduction

Prominent iron accumulation in the brain was associated with rare hereditary neurodegeneration with brain iron accumulation (NBIA) disorders, in which iron built-up in the brain could be detected in the first decade of young cases [1]. Hereditary NBIAs consisted of more than ten clinical subtypes caused by different genetic defects, most of which were associated with mutations in loci of WDR45, PANK2, or PLA2G6 [2]. Recent studies identified mutations in C19orf12 gene in a novel NBIA subtype termed as mitochondrial membrane protein-associated neurodegeneration (MPAN) due to the mitochondrial membrane localization of wild-type C19orf12 protein [3]. Like other NBIA types, MPAN was characterized by the massive accumulation of iron and aggressive neurodegeneration in the brain, particularly in basal ganglia, among affected cases diagnosed with devastating neurological symptoms [4]. Most MPAN cases showed autosomal recessive heredity, while some C19orf12 mutants display dominant transmission likely due to dominant-negative effects of these mutations, suggesting a loss of function mechanism in the pathogenesis of MPAN [5, 6]. Highly conserved among vertebrates, C19orf12 gene encodes an orphan mitochondrial membrane protein while the function of the protein and the pathogenic mechanism of its mutations underlying neurodegeneration in MPAN remain elusive [7-9].

In the central nervous system, iron metals are involved in many important physiological processes such as mitochondrial respiration, DNA replication, neurotransmitter synthesis

and myelin formation [10]. On the other hand, iron accumulation could cause oxidative damage to biomolecules because of the redox reactivity of iron atoms. Therefore, iron levels are strictly controlled [11]. Aberrant iron regulation in the brain is associated with oxidative damage characterizing multiple common neurodegenerative diseases such as Alzheimer's disease and Parkinson's diseases[12, 13]. Emerging evidence suggested that overload of cellular pool of redox active iron could initiate ferroptosis, a regulated cell death that is biochemically and genetically distinct from other regulated cell death such as apoptosis [14, 15]. Indeed, ferroptosis was one common cause of regulated and progressive cell death in multiple neurodegenerative disorders including neuronal loss related to the neuronal toxicity of glutamate [16], intracerebral hemorrhage [17], amyotrophic lateral sclerosis [18], and Parkinson's diseases [19]. Mitochondria play a critical role in the regulation of iron metabolism and importantly ferroptosis was closely associated with impaired mitochondrial homeostasis [20]. Given the massive iron accumulation in the brain of MPAN cases and mitochondrial localization of C19orf12, it is of interest to determine whether ferroptosis is involved in neuronal dysfunction and cell death during the pathogenesis of MPAN and whether and how C19orf12 mutations impact mitochondria and iron regulation. To address these important gaps in our knowledge, we investigated cellular models and biopsied brain tissues of MPAN for mitochondria deficits, iron changes, oxidative stress and ferroptosis.

Material and methods

Cell culture and MPAN tissue

Biopsy cortical tissue of a C19orf12^{T11M} MPAN case was collected and reported previously [21]. Normal control samples were obtained from the Case Western Reserve Brain Bank. Human neuroblastoma M17 cells were maintained in OptiMEM supplemented with 1% Penicillin and Streptomycin and 5% FBS (Gibco) in incubator with 5% CO_2at 37 °C. Three lines of C19orf12 KO M17 cells were generated by crisper-cas9 by targeting sequence: CGCCACGATGACTATCATGG (Abm). Primary skin fibroblasts of MPAN cases (bearing C19orf12$^{G58S/G58S}$ or heterozygous C19orf12^{p99fs*102}) were obtained from EuroBioBank and were cultured in DMEM with 1% Penicillin and 10% FBS supplemented with essential amino acids (Invitrogen). The gender and age matched control of skin fibroblasts were obtained from Coriell Institute. C19orf12 cDNA was obtained from Addgene and cloned into pCMV-lenti vector (Clontech). Mitochondria was visualized by mitoDsRed transfection as previously described [22]. Plasmids were transfected with Lipofectamine 2000 reagent.

Live cell imaging with fluorescent probes

Cells were seeded in glass bottom 35 mm dishes (Ibidi) with density of 0.5 million cells per well for 24 hours. Cells were loaded with fluorescent probes to measure cytosolic labile ferrous iron (BioTracker 575 Red Fe^{2+} Dye, Millipore), cytosolic labile iron (Calcein-AM, Thermo), lipid peroxidation (BODIPY™ 581/591 C11, Thermo), cytosolic ROS (H2DCFDA, Thermo) and mitochondrial ROS (mitoSOX, Thermo). Dyes were incubated with cells for 15~30 minutes and washed with warmed PBS for three times. Cells were treated by Erastin or RSL3 (Cayman) overnight and cell death were analyzed by propidium iodide (PI) (Sigma) staining for 15 minutes. Live cell images were collected by Plan-Apo 20x/0.8 objective and Axiocam 503 Mono camera with AxioVert 200 system.

Cellular fractionation and oxygen consumption assay

Mitochondria were purified as previously described [23]. Briefly, cells were homogenized with MSM (220mM D-mannitol, 70mM sucrose, 5mM MOPS, pH 7.4) by 2 ml Dounce homogenizer. Homogenates were centrifuged at 500g for 10 minutes and the supernatants were further centrifuged at 9000g for 10 mins to obtain mitochondrial fraction in the pellets. Total cell homogenates were subject to 270,000g centrifugation to obtain cytosolic (supernatant) and membrane fractions (pellet). Mitochondrial respiration in cultured cells were analyzed by Seahorse XF-24 analyzer (Seahorse Bioscience) as described before [22]. Cells were seeded in plates at a density of 100,000 cells per well which was coated with poly-D lysine (50 μg/ml). The assay protocol consisted of repeated cycles of 3 minutes mixing, 2 minutes wait and 3 minutes measurement periods. Basal OCR was measured 3 times before drug exposure. Then oligomycin (1 μM), FCCP (0.5 μM for M17 cells and 2 μM for primary fibroblasts) and Rotenone/antimycin A (0.5 μM) were injected sequentially. After injection of each drug, OCR measurements were made three times.

ATP and iron measurement

Cellular ATP levels were measured by luminescence methods with cell homogenates as described in the kit instructions (Cayman) and measured by Biotek Synergy H1. For total iron level measurement, mitochondria and cytosol fractions were digested with equal volume of concentrated trace-metal grade nitric acid. The samples were heated for 2 hours at 90 °C and were assayed for iron levels by atomic absorption spectroscopy.

SDS-PAGE and western blot

SDS-PAGE and western blot were performed as we previously published [24]. Cells were lysed by NP-40 cell lysis buffer (50 mM Tris, pH 7.4, 250 mM NaCl ,5 mM EDTA, 50 mM NaF, 1 mM Na_3CO_4 and 1 % NP40) with 1X protease inhibitor cocktail (Cell signaling) and were centrifuged at 18,000 g at 4°C for 30 minutes. Samples were separated by 4–12% Bis-Tris Protein Gel (Bio-rad) and blotted to PVDF membrane. The blots were probed with primary and secondary antibodies at room temperature for 1-2 hours and then imaged by Amersham Imager 600 imager. Antibodies used in the study were C19orf12 (27382, Proteintech), VDAC (10866, Proteintech), Actin (66009, Proteintech), HMOX1 (SPA-895, Enzo Life Sciences), 8OHG (12501, QED Bioscience) and HNE (HNE11-S, Alpha Diagnostics Intl).

Immunocytochemistry, confocal immunofluorescence and EM

Cells were seeded on the 12 mm NO.1.5 round cover glass 24 hours before transfection. 48 hours after transfection, cells were fixed in 4% fresh paraformaldehyde for 10 minutes at room temperature and washed with PBS three times. Fixed cells were permeabilized with 0.5% Triton X-100 and blocked with 10% NGS for 30 minutes at room temperature, then incubated with primary antibody overnight at cold room and then incubated with fluor-conjugated secondary antibody (Thermo) at room temperature for 1 hour. The sections were mounted on the top of glass slide with Fluoromount-G mounting medium (Southern Biotech). Confocal images were collected by Leica TSC S8 platform with an inverted DMI 6000 adaptive focus microscope. Immunocytochemistry was performed by the peroxidase

anti-peroxidase protocol with formalin fixed paraffin embedded brain samples sectioned at 6 μm thickness as described before [23]. For electron microscopic images, cultured cells were treated with EM fixative (the quarter strength Karnovsky–1.25% DMSO mixture). Then specimens were dehydrated in ascending concentrations of ethanol and embedded in Poly/Bed 812 embedding resin (Polysciences, Warrington, PA, USA). Thin sections were sequentially stained with 2% acidified uranyl acetate followed by Sato's triple lead staining and examined in an FEI Tecnai T12 electron microscope equipped with a Gatan single tilt holder and a CCD camera (Gatan, Pleasanton, CA, USA).

Statistical analysis

All these data were independently assessed by investigators without prior knowledge of samples. Statistical analysis was done with one-way or two-way analysis of variance (ANOVA) followed by multiple comparison test or Student's t-test. Data were normally distributed with similar variance between the groups.

Results

Loss of C19orf12 caused mitochondrial dysfunction in M17 cells.

It was suggested that MPAN-associated C19orf12 mutations caused either loss of function through the recessive inheritance of C19orf12 mutations (e.g., T11M and G58S mutations), or through dominant-negative effects in individuals with only one heterozygous mutation such as p99fs*102 [5, 6]. Therefore, we established stable M17 cell lines to abolish protein expression of C19orf12 (i.e., C19orf12 KO cell lines) with CRISPR-Cas9 technique as cell models of MPAN. Western blot analysis with C19orf12 antibody showed non-detectable C19orf12 protein in C19orf12 KO cells when compared with wildtype (WT) M17 cells (Fig 1A). Given the mitochondrial localization of C19orf12 protein, we first determined the effects on mitochondria in C19orf12 KO cells. Mitochondrial morphology was visualized by confocal fluorescent images after transient transfection of mitoDsRed (Fig 1B). There was significant reduction of mitochondrial length in C19orf12 KO M17 cells compared with WT M17 cells. Mitochondrial function was determined by seahorse assay which revealed impaired mitochondrial respiration activity in C19orf12 KO M17 cells as evidenced by significantly reduced maximal oxygen consumption rate (OCR) (Fig 1D-E). It was noted that non-mitochondrial respiration was increased in C19orf12 KO M17 cells (Fig 1G). Collectively, these data demonstrated that loss of C19orf12 caused mitochondrial deficits in neurons.

Loss of C19orf12 increased iron levels and oxidative stress damages in lipids in M17 cells.

MPAN is characterized by massive iron accumulation in cerebral tissues [4]. We hypothesized that loss of C19orf12 protein might affect cellular iron pool to disturb cellular homeostasis. To test this hypothesis, the labile iron pool was analyzed with two specific cellular iron probes BioTracker 575 and Calcein-AM. Live cell imaging revealed that BioTracker 575 fluorescence was increased while Calcein-AM was quenched following chelation of low-mass labile iron, suggesting both cytosolic ferrous and ferric iron pools were increased in C19orf12 KO cells (Fig 2A-B). To corroborate this finding, total iron levels were analyzed by atomic furnace spectrometry in the cytosolic and mitochondrial fractions isolated from

C19orf12 KO cells. Iron levels were significantly increased in cytosol fraction of C19orf12 KO cells, though the iron levels in mitochondrial fraction were decreased but did not reach significance in C19orf12 KO cells (Fig 2C). Increased cellular transition metals such as iron promotes generation of reactive oxygen species (ROS) [25]. In this regard, cytosolic ROS and mitochondrial ROS were measured by fluorescent probes H2DCFDA and mitoSOX in live cells (Fig 2D). Consistent with increased iron levels in the cytosol but not in mitochondria, there were significantly increased ROS levels in the cytosol but no changes of ROS levels in the mitochondria in C19orf12 KO cells. Accompanying the increased cytosolic ROS, lipid peroxidation levels measured by BODIPY C11 for probe by live cell imaging showed significant increase of oxidized membrane lipids in C19orf12 KO cells (Fig 2E), suggesting impaired membrane integrity of cellular organelles in cells with loss of C19orf12 proteins.

Antioxidant treatment rescued oxidative damage and mitochondrial dysfunction in C19orf12 KO cells

To determine the causal role of oxidative stress on mitochondrial dysfunction in the C19orf12 KO cells, these cells were treated with a widely used antioxidant, n-acetyl cysteine (NAC, 5mM). Interestingly, NAC treatment significantly rescued mitochondrial fragmentation in C19orf12 KO cells as evidenced by increased mitochondrial length (Fig 3A). NAC treatment also rescued mitochondrial function in C19orf12 KO cells as evidenced by improved maximal OCR and ATP production (Fig 3B and C). More importantly, NAC treatment could attenuate levels of lipid ROS measured by BODIPY C11 probe in live cells or isolated mitochondria from C19orf12 KO cell (Fig 3D). These data suggested the essential role of oxidative stress in mediating the toxic effects of C19orf12 ablation on mitochondrial structure and function in MPAN.

Loss of C19orf12 caused increased vulnerability to ferroptosis in M17 cells.

Given the increased iron overload and lipid peroxidation in C19orf12 KO cells, we hypothesized that C19orf12 KO cells might be susceptible to ferroptosis. To test this hypothesis, C19orf12 KO cells or WT control M17 cells were treated with erastin for 24-hours to induce ferroptosis (Fig 4A). As expected, erastin induced significant cell death in WT control cells in a dose-dependent manner. However, significantly greater cell death was induced by erastin in C19orf12 KO cells at all concentrations compared with WT control cells. GPX4 inhibitor RSL3 was also used to induce ferroptosis and similarly, C19orf12 KO cells demonstrated significantly greater cell death after RSL treatment compared with WT control cells (Fig 4B).

The iron chelator desferoxamine (DFO) has been shown to inhibit ferroptosis [26]. Indeed, erastin-induced cell death was completely inhibited by DFO pretreatment in both WT control cells and C19orf12 KO cells (Fig 4C). Notably, following DFO treatment, levels of lipid ROS in C19orf12 KO cells were comparable to WT control cells (Fig 4D). Moreover, DFO treatment also rescued mitochondrial fragmentation (Fig 4E) and mitochondrial function measured by ATP levels and mitochondrial maximal respiration (Fig 4F-G) in C19orf12 KO cells.

Increased iron level and ferroptosis in human MPAN skin fibroblasts

To determine whether pathogenic C19orf12 mutations caused mitochondrial and iron deficits, primary cultures of skin fibroblasts derived from the skin biopsies of two MPAN cases bearing C19orf12$^{G58S/G58S}$ or heterozygous C19orf12^{p99fs*102} mutations were compared with age- and gender- matched normal control cells. We first analyzed changes of mitochondrial morphology and function. Consistent with the findings in C19rof12 KO M17 cells, electron microscopy and quantitative analysis revealed significantly reduced mitochondrial length in C19orf12^{G58S} MPAN skin fibroblasts compared with normal controls (Fig 5A). Furthermore, mitochondrial oxygen consumption rate (OCR) assays demonstrated impaired mitochondrial respiratory function as evidenced by significantly reduced basal OCR, ATP production linked OCR and maximal OCR in C19orf12$^{G58S/G58S}$ and C19orf12^{p99fs*102} MPAN skin fibroblasts (Fig 5B-E).

We next analyzed live cultures of human MPAN skin fibroblasts with iron fluorescent probes. Indeed, the levels of cytosolic labile ferrous iron (Figure 6A) and total cytosolic labile iron (Figure 6B) were significantly increased in MPAN skin fibroblasts bearing either homozygous C19orf12^{G58S} or heterozygous C19orf12^{p99fs*102} mutations when compared with normal control fibroblasts. Lipid ROS levels indicated by fluorescent BODIPY C11 probes were also increased in MPAN skin fibroblasts bearing either homozygous C19orf12^{G58S} or C19orf12^{p99fs*102} mutations (Fig 6C). These data suggested that C19orf12 mutations caused mitochondrial deficits, iron overload and lipid peroxidation in patient fibroblast cells.

To determine whether patient fibroblasts were vulnerable to ferroptosis, these cells were treated with 25 μM erastin for 24 hours and cell death was measured by PI uptake. Indeed, erastin induced significantly more PI decorated dead cells in MPAN skin fibroblasts bearing either homozygous C19orf12^{G58S} or C19orf12^{p99fs*102} mutations when compared with control cells. Importantly, erastin-induced cell death in MPAN skin fibroblasts was almost completely abolished by the pretreatment of iron chelator DFO (Fig 6D). In fact, DFO treatment also rescued cytosolic ROS levels (Fig 6E) and mitochondrial function measured by ATP levels (Fig 6F) in C19orf12^{G58S} or C19orf12^{p99fs*102} mutations fibroblasts.

Mitochondria deficits and ferroptosis related oxidative damages in the MPAN brain.

To determine whether mitochondrial deficits and ferroptosis-related mechanism may be involved in the brain of MPAN patients, biopsied cortical tissue of MPAN case with C19orf12^{T11M} mutation was analyzed. Mitochondrial morphology was analyzed by immunofluorescent microscopy with antibody cocktail against OXPHOS proteins and compared with biopsied cortical tissues from age-matched controls. Confocal images showed normal filament-like mitochondria in cortical neurons in the control sample. In contrast, mitochondria became fragmented in neurons of MPAN case bearing C19orf12^{T11M} mutation (Fig 7A). Indeed, quantification analysis revealed significantly reduced mitochondrial length in MPAN case, indicative of mitochondrial fragmentation. Furthermore, there was reduced coverage of mitochondria in the neuronal somas, as evidenced by the remarkable reduction of neuronal mitochondrial index in MPAN with C19orf12^{T11M} mutation (Figure 7A). To explore the likely role of ferroptosis in MPAN

C19orf12^{T11M} brain, we focused on ferroptosis related oxidative damages in cortical neurons. We analyzed the protein expression of HMOX1 (also known as HO-1), an antioxidant protein induced by oxidative stress which is widely used as an oxidative stress and ferroptosis marker [27]. Notably, neuronal expression of HMOX1 in C19orf12^{T11M} case was significantly increased compared with that in control samples (Fig 7B). Importantly, there was increased lipid peroxidation detected by 4-HNE and DNA oxidation detected by 8-OHG in cortical neurons in the MPAN case (Fig 7C-D). Taken together, MPAN neurons demonstrated remarkable mitochondrial deficit and ferroptosis associated oxidative damages.

Discussion

In this study, we established C19orf12 knockout M17 human neuroblastoma cell lines as a cell model of MPAN and characterized MPAN-related cellular defects in this model. As a mitochondrial membrane protein [3], C19orf12 ablation caused mitochondrial fragmentation and functional deficits in M17 neurons. MPAN is characterized by iron accumulation in the brain [4], and in this study C19orf12 ablation indeed caused dramatic iron overload in M17 neurons which was accompanied by significantly increased cytosolic ROS generation and lipid peroxidation. Moreover, we found C19orf12 ablation led to increased neuronal susceptibility to erastin- or RSL3-induced ferroptosis. Interestingly, these defects induced by C19orf12 ablation could be rescued by DFO, an iron chelator. By using fibroblasts from MPAN patients carrying two different C19orf12 mutations as an additional cell model of MPAN, we confirmed that C19orf12 mutants caused mitochondrial defects, iron overload, lipid peroxidation and increased susceptibility to ferroptosis which could also be rescued by DFO. Importantly, we provided further evidence demonstrating mitochondrial deficits and increased oxidative stress and lipid peroxidation in the biopsied brain from MPAN patients. These data support the contribution of ferroptosis mechanism to neurodegeneration in MPAN and suggest the critical role of iron overload in mitochondrial dysfunction and neurodegeneration in the pathogenesis of MPAN.

Although characteristic iron accumulation was found in the parenchyma of MPAN patients [4], it remains elusive whether and how iron accumulation plays a role in neurodegeneration and pathogenesis of MPAN. We first investigated whether C19orf12 ablation in neurons caused any abnormal changes in the labile iron pool (LIP), a subset of intracellular iron which readily participate in redox cycling [25]. The data unveiled robust and remarkable increases of both ferrous and ferric iron levels in the LIP in C19orf12 KO cells and skin fibroblast from MPAN patients which appears due to significant changes in the cytosolic LIP It was interesting to note that there was no remarkable change of LIP in mitochondria in these MPAN cell models. This is likely due to the limited storage capacity and LIP within neuronal mitochondria [28]. Excessive labile iron usually led to dramatic oxidative damages in the cell [25]. Indeed, there were increased ROS levels and lipid peroxidation damages in both C19orf12 knockout neurons and MPAN fibroblasts. Mitigation of iron levels by iron chelator alleviated oxidative damages in these MPAN cell models, confirming the dependence of oxidative damages on increased iron levels in MPAN neurons. Importantly, we confirmed extensive oxidative damage to lipid and protein in neurons in the biopsied MPAN brain tissues, which suggests iron overload likely contributed to oxidative damages in the brain,

thus supporting a critical pathogenic role of iron overload in the MPAN pathogenesis. Iron overload and lipid peroxidation have been associated with ferroptosis [25]. Indeed, we found that C19orf12 KO M17 neurons and MPAN fibroblasts were sensitive to ferroptosis when cells were challenged by erastin or RSL3, both are well known to chemically induce the ferroptosis pathway. These findings suggest an important role of ferroptosis in the neurodegeneration of MPAN. Emerging evidence demonstrated that ferroptosis is involved in several related neurodegenerative diseases including Parkinson disease and Alzheimer's disease[29] where both iron accumulation and lipid peroxidation were also present. Importantly, iron chelator DFP could almost completely rescue erastin-induced cell death in both C19orf12 KO M17 cells and MPAN fibroblasts, again highlighting the crucial role of iron overload that triggered a cascade of toxic events through lipid peroxidation to eventual cell death. It remains to be determined how C19orf12 changes caused iron overload. We found increased HMOX1 expression in the biopsied cortical tissue from MPAN patient, suggesting that an altered heme metabolism may be involved which warrants further investigation.

Mitochondria are critical for neuronal function and survival [30]. C91orf12 was originally identified as a mitochondrial membrane protein, however, it was not clear whether and how mitochondrial dysfunction is involved in the pathogenesis of MPAN caused by C19orf12 mutations. We found dramatic mitochondrial fragmentation accompanied by significantly impaired mitochondrial respiratory function and ATP generation in the C19orf12 KO M17 cells and MPAN fibroblasts. The rescue of mitochondrial fragmentation by NAC or DFO treatment led to the rescue of mitochondrial function suggesting that loss of C19orf12 function caused oxidative stress leading to mitochondrial fragmentation which in turn mediated mitochondrial dysfunction. In fact, both oxidative stress and mitochondrial fragmentation were also found in the biopsied cortical brain tissues from MPAN patients, suggesting that mitochondrial dysfunction is likely involved in MPAN disease. Prior studies demonstrated that mitochondrial dysfunction was involved in some subset of NBIA [31], our study suggests a more common role of mitochondrial dysfunction in the pathogenesis of NBIA. It is of interest to note that the observation of mitochondrial fragmentation mediated mitochondrial dysfunction was extensively reported in different neurodegenerative diseases such as Alzheimer's disease and Parkinson's disease[30, 32, 33] and unopposed mitochondrial fission caused neurodegeneration in multiple brain areas [34-36]. How did C19orf12 changes cause mitochondrial fragmentation? It was suggested that the altered polarity and shape of phospholipid peroxidation products could change the properties of membrane and related membrane fusion events [37]. Given the increased lipoperoxidation of membrane in C19orf12 cells, the fusion of mitochondrial membranes was likely insulted by the buildup of oxidized lipids on mitochondrial membranes. Indeed, our study showed that antioxidant NAC treatment not only could prevent the lipoperoxidation buildup but also restore the mitochondrial fusion in C19orf12 cells, suggesting the essential role of enhanced lipid oxidation on mitochondrial membrane fusion and fission. In addition to these changes of phospholipid membranes, our unshown findings also demonstrated C19orf12 ablation caused increased expression of DLP1, an essential mitochondrial fission factor but no changes in the expression of mitochondrial fusion GTPases such as Mfn2 and OPA1, suggesting excessive fission likely plays a role as well. It was recently reported that

C19orf12 was localized to ER-mitochondrial contact sites [7, 38], it is possible that C19orf12 changes may also cause excessive mitochondrial fission through disturbed ER-mitochondria interaction or perturbed mitochondrial calcium handling. Because no cell death was observed at basal conditions in the C19orf12 KO cells or MPAN fibroblasts, it may suggest that mitochondrial fragmentation and dysfunction were not caused by ferroptosis. However, the lack of cell death in our MPAN cell culture system *in vitro* may be due to longer incubation time required for cell death events *in vivo* as observed in human MPAN patients. Compared with low oxygen levels in neurons *in vivo*, the enhanced antioxidant mechanisms and cellular adaptation to increased oxidative stress in common cell culture models could mitigate the ferroptosis related damages in cultured neurons *in vitro*. Future studies should address these limitations in this study with a MPAN experimental model in vivo. Nevertheless, given that fragmented mitochondria and mitochondrial dysfunction could lead to increased ROS generation and oxidative damage [30], they could exacerbate iron overload-induced oxidative stress and contribute to ferroptosis and neurodegeneration in MPAN[34, 39]. It is of interest to note that emerging evidence suggested crosstalk between mitochondrial function and ferroptosis in cell. For example, it was reported that mitochondrial metabolites of TCA cycle directly regulated ferroptosis [40], and dihydroorotate dehydrogenase (DHODH) in mitochondrial attenuated lipid peroxidation to guard cell from ferroptosis [41]. Therefore, more detailed studies into the role of mitochondrial fragmentation and dysfunction in C19orf12 changes induced-ferroptosis and neurodegeneration in MPAN pathogenesis are warranted.

Conclusion

Taken together, this study demonstrated loss of C19orf12 function caused iron overload, lipid peroxidation and susceptibility to ferroptosis which likely plays an important role in neurodegeneration and the pathogenesis of MPAN. Such characteristic susceptibility of ferroptosis was associated with mitochondrial fragmentation and functional deficits in affected MPAN cells. Manipulation of cellular stress burden by antioxidants or iron chelators could alleviate mitochondrial dysfunction and prevent cell death in MPAN cells. These findings provide a new framework for future mechanistic studies into the understanding of neurodegeneration in MPAN which may generate novel therapeutic targets for the disease.

Acknowledgement

The work was supported in part by the National Institutes of Health [R03AG063362 and R03NS112782 to W.W.]. W.W. was a program participant in the Research Education Component of the Cleveland Alzheimer's Disease Research Center supported by NIA P30 AG062428 and AG072959.

Reference

1. Meyer E, Kurian MA, Hayflick SJ. Neurodegeneration with Brain Iron Accumulation: Genetic Diversity and Pathophysiological Mechanisms. Annu Rev Genomics Hum Genet. 2015;16:257–79. Epub 2015/05/15. doi: 10.1146/annurev-genom-090314-025011. PubMed PMID: 25973518. [PubMed: 25973518]

2. Levi S, Tiranti V. Neurodegeneration with Brain Iron Accumulation Disorders: Valuable Models Aimed at Understanding the Pathogenesis of Iron Deposition. Pharmaceuticals (Basel). 2019;12(1). Epub 2019/02/13. doi: 10.3390/ph12010027. PubMed PMID: 30744104; PMCID: PMC6469182.
3. Hartig MB, Iuso A, Haack T, Kmiec T, Jurkiewicz E, Heim K, Roeber S, Tarabin V, Dusi S, Krajewska-Walasek M, Jozwiak S, Hempel M, Winkelmann J, Elstner M, Oexle K, Klopstock T, Mueller-Felber W, Gasser T, Trenkwalder C, Tiranti V, Kretzschmar H, Schmitz G, Strom TM, Meitinger T, Prokisch H. Absence of an orphan mitochondrial protein, c19orf12, causes a distinct clinical subtype of neurodegeneration with brain iron accumulation. Am J Hum Genet. 2011;89(4):543–50. Epub 2011/10/11. doi: 10.1016/j.ajhg.2011.09.007. PubMed PMID: 21981780; PMCID: PMC3188837. [PubMed: 21981780]
4. Gregory A, Klopstock T, Kmiec T, Hogarth P, Hayflick SJ. Mitochondrial Membrane Protein-Associated Neurodegeneration. In: Adam MP, Ardinger HH, Pagon RA, Wallace SE, Bean LJH, Gripp KW, Mirzaa GM, Amemiya A, editors. GeneReviews(®). Seattle (WA): University of Washington, Seattle Copyright © 1993-2021, University of Washington, Seattle. GeneReviews is a registered trademark of the University of Washington, Seattle. All rights reserved.; 1993.
5. Monfrini E, Melzi V, Buongarzone G, Franco G, Ronchi D, Dilena R, Scola E, Vizziello P, Bordoni A, Bresolin N, Comi GP, Corti S, Di Fonzo A. A de novo C19orf12 heterozygous mutation in a patient with MPAN. Parkinsonism Relat Disord. 2018;48:109–11. Epub 2018/01/04. doi:10.1016/j.parkreldis.2017.12.025. PubMed PMID: 29295770. [PubMed: 29295770]
6. Gregory A, Lotia M, Jeong SY, Fox R, Zhen D, Sanford L, Hamada J, Jahic A, Beetz C, Freed A, Kurian MA, Cullup T, van der Weijden MCM, Nguyen V, Setthavongsack N, Garcia D, Krajbich V, Pham T, Woltjer R, George BP, Minks KQ, Paciorkowski AR, Hogarth P, Jankovic J, Hayflick SJ. Autosomal dominant mitochondrial membrane protein-associated neurodegeneration (MPAN). Mol Genet Genomic Med. 2019;7(7):e00736. Epub 2019/05/16. doi: 10.1002/mgg3.736. PubMed PMID: 31087512; PMCID: PMC6625130. [PubMed: 31087512]
7. Venco P, Bonora M, Giorgi C, Papaleo E, Iuso A, Prokisch H, Pinton P, Tiranti V. Mutations of C19orf12, coding for a transmembrane glycine zipper containing mitochondrial protein, cause mislocalization of the protein, inability to respond to oxidative stress and increased mitochondrial Ca^{2+}. Front Genet. 2015;6:185. Epub 2015/07/03. doi: 10.3389/fgene.2015.00185. PubMed PMID: 26136767; PMCID: PMC4470416. [PubMed: 26136767]
8. Iuso A, Sibon OC, Gorza M, Heim K, Organisti C, Meitinger T, Prokisch H. Impairment of Drosophila orthologs of the human orphan protein C19orf12 induces bang sensitivity and neurodegeneration. PLoS One. 2014;9(2):e89439. Epub 2014/03/04. doi: 10.1371/journal.pone.0089439. PubMed PMID: 24586779; PMCID: PMC3931782. [PubMed: 24586779]
9. Mignani L, Zizioli D, Borsani G, Monti E, Finazzi D. The Downregulation of c19orf12 Negatively Affects Neuronal and Musculature Development in Zebrafish Embryos. Front Cell Dev Biol. 2020;8:596069. Epub 2021/01/12. doi: 10.3389/fcell.2020.596069. PubMed PMID: 33425903; PMCID: PMC7785858. [PubMed: 33425903]
10. Muckenthaler MU, Rivella S, Hentze MW, Galy B. A Red Carpet for Iron Metabolism. Cell. 2017;168(3):344–61. Epub 2017/01/28. doi: 10.1016/j.cell.2016.12.034. PubMed PMID: 28129536; PMCID: PMC5706455. [PubMed: 28129536]
11. Rouault TA. Iron metabolism in the CNS: implications for neurodegenerative diseases. Nat Rev Neurosci. 2013;14(8):551–64. Epub 2013/07/04. doi: 10.1038/nrn3453. PubMed PMID: 23820773. [PubMed: 23820773]
12. Ward RJ, Zucca FA, Duyn JH, Crichton RR, Zecca L. The role of iron in brain ageing and neurodegenerative disorders. Lancet Neurol. 2014;13(10):1045–60. Epub 2014/09/19. doi:10.1016/s1474-4422(14)70117-6. PubMed PMID: 25231526; PMCID: PMC5672917. [PubMed: 25231526]
13. Benarroch EE. Brain iron homeostasis and neurodegenerative disease. Neurology. 2009;72(16):1436–40. Epub 2009/04/22. doi: 10.1212/WNL.0b013e3181a26b30. PubMed PMID: 19380704. [PubMed: 19380704]
14. Li J, Cao F, Yin HL, Huang ZJ, Lin ZT, Mao N, Sun B, Wang G. Ferroptosis: past, present and future. Cell Death Dis. 2020;11(2):88. Epub 2020/02/06. doi: 10.1038/s41419-020-2298-2. PubMed PMID: 32015325; PMCID: PMC6997353. [PubMed: 32015325]

15. Jiang X, Stockwell BR, Conrad M. Ferroptosis: mechanisms, biology and role in disease. Nat Rev Mol Cell Biol. 2021;22(4):266–82. Epub 2021/01/27. doi: 10.1038/s41580-020-00324-8. PubMed PMID: 33495651; PMCID: PMC8142022. [PubMed: 33495651]

16. Stockwell BR, Friedmann Angeli JP, Bayir H, Bush AI, Conrad M, Dixon SJ, Fulda S, Gascon S, Hatzios SK, Kagan VE, Noel K, Jiang X, Linkermann A, Murphy ME, Overholtzer M, Oyagi A, Pagnussat GC, Park J, Ran Q, Rosenfeld CS, Salnikow K, Tang D, Torti FM, Torti SV, Toyokuni S, Woerpel KA, Zhang DD. Ferroptosis: A Regulated Cell Death Nexus Linking Metabolism, Redox Biology, and Disease. Cell. 2017;171(2):273–85. Epub 2017/10/07. doi: 10.1016/j.cell.2017.09.021. PubMed PMID: 28985560; PMCID: PMC5685180. [PubMed: 28985560]

17. Wan J, Ren H, Wang J. Iron toxicity, lipid peroxidation and ferroptosis after intracerebral haemorrhage. Stroke Vasc Neurol. 2019;4(2):93–5. Epub 2019/07/25. doi: 10.1136/svn-2018-000205. PubMed PMID: 31338218; PMCID: PMC6613877. [PubMed: 31338218]

18. Chen L, Na R, Danae McLane K, Thompson CS, Gao J, Wang X, Ran Q. Overexpression of ferroptosis defense enzyme Gpx4 retards motor neuron disease of SOD1G93A mice. Sci Rep. 2021;11(1):12890. Epub 2021/06/20. doi: 10.1038/s41598-021-92369-8. PubMed PMID: 34145375; PMCID: PMC8213805. [PubMed: 34145375]

19. Angelova PR, Choi ML, Berezhnov AV, Horrocks MH, Hughes CD, De S, Rodrigues M, Yapom R, Little D, Dolt KS, Kunath T, Devine MJ, Gissen P, Shchepinov MS, Sylantyev S, Pavlov EV, Klenerman D, Abramov AY, Gandhi S. Alpha synuclein aggregation drives ferroptosis: an interplay of iron, calcium and lipid peroxidation. Cell Death Differ. 2020;27(10):2781–96. Epub 2020/04/29. doi: 10.1038/s41418-020-0542-z. PubMed PMID: 32341450; PMCID: PMC7492459. [PubMed: 32341450]

20. Wang H, Liu C, Zhao Y, Gao G. Mitochondria regulation in ferroptosis. Eur J Cell Biol. 2020;99(1):151058. Epub 2019/12/08. doi: 10.1016/j.ejcb.2019.151058. PubMed PMID: 31810634. [PubMed: 31810634]

21. Gore E, Appleby BS, Cohen ML, DeBrosse SD, Leverenz JB, Miller BL, Siedlak SL, Zhu X, Lerner AJ. Clinical and imaging characteristics of late onset mitochondrial membrane protein-associated neurodegeneration (MPAN). Neurocase. 2016;22(5):476–83. Epub 2016/11/02. doi: 10.1080/13554794.2016.1247458. PubMed PMID: 27801611; PMCID: PMC5568540. [PubMed: 27801611]

22. Wang W, Ma X, Zhou L, Liu J, Zhu X. A conserved retromer sorting motif is essential for mitochondrial DLP1 recycling by VPS35 in Parkinson's disease model. Hum Mol Genet. 2017;26(4):781–9. Epub 2017/01/04. doi: 10.1093/hmg/ddw430. PubMed PMID: 28040727; PMCID: PMC5903416. [PubMed: 28040727]

23. Wang W, Yin J, Ma X, Zhao F, Siedlak SL, Wang Z, Torres S, Fujioka H, Xu Y, Perry G, Zhu X. Inhibition of mitochondrial fragmentation protects against Alzheimer's disease in rodent model. Hum Mol Genet. 2017;26(21):4118–31. Epub 2017/10/04. doi: 10.1093/hmg/ddx299. PubMed PMID: 28973308; PMCID: PMC5886251. [PubMed: 28973308]

24. Zhao F, Xu Y, Gao S, Qin L, Austria Q, Siedlak SL, Pajdzik K, Dai Q, He C, Wang W, O'Donnell JM, Tang B, Zhu X. METTL3-dependent RNA m(6)A dysregulation contributes to neurodegeneration in Alzheimer's disease through aberrant cell cycle events. Mol Neurodegener. 2021;16(1):70. Epub 2021/10/02. doi: 10.1186/s13024-021-00484-x. PubMed PMID: 34593014; PMCID: PMC8482683. [PubMed: 34593014]

25. Kakhlon O, Cabantchik ZI. The labile iron pool: characterization, measurement, and participation in cellular processes(1). Free Radic Biol Med. 2002;33(8):1037–46. Epub 2002/10/11. doi: 10.1016/s0891-5849(02)01006-7. PubMed PMID: 12374615. [PubMed: 12374615]

26. Floros KV, Cai J, Jacob S, Kurupi R, Fairchild CK, Shende M, Coon CM, Powell KM, Belvin BR, Hu B, Puchalapalli M, Ramamoorthy S, Swift K, Lewis JP, Dozmorov MG, Glod J, Koblinski JE, Boikos SA, Faber AC. MYCN-Amplified Neuroblastoma Is Addicted to Iron and Vulnerable to Inhibition of the System Xc-/Glutathione Axis. Cancer Res. 2021;81(7):1896–908. Epub 2021/01/24. doi: 10.1158/0008-5472.Can-20-1641. PubMed PMID: 33483374. [PubMed: 33483374]

27. Tang Z, Ju Y, Dai X, Ni N, Liu Y, Zhang D, Gao H, Sun H, Zhang J, Gu P. HO-1-mediated ferroptosis as a target for protection against retinal pigment epithelium degeneration. Redox Biol.

2021;43:101971. Epub 20210417. doi: 10.1016/j.redox.2021.101971. PubMed PMID: 33895485; PMCID: PMC8099560. [PubMed: 33895485]

28. Horowitz MP, Greenamyre JT. Mitochondrial iron metabolism and its role in neurodegeneration. J Alzheimers Dis. 2010;20 Suppl 2(Suppl 2):S551–68. Epub 2010/05/14. doi: 10.3233/jad-2010-100354. PubMed PMID: 20463401; PMCID: PMC3085540. [PubMed: 20463401]
29. Reichert CO, de Freitas FA, Sampaio-Silva J, Rokita-Rosa L, Barros PL, Levy D, Bydlowski SP. Ferroptosis Mechanisms Involved in Neurodegenerative Diseases. Int J Mol Sci. 2020;21(22). Epub 2020/11/26. doi: 10.3390/ijms21228765. PubMed PMID: 33233496; PMCID: PMC7699575.
30. Wang W, Zhao F, Ma X, Perry G, Zhu X. Mitochondria dysfunction in the pathogenesis of Alzheimer's disease: recent advances. Mol Neurodegener. 2020;15(1):30. Epub 2020/05/31. doi: 10.1186/s13024-020-00376-6. PubMed PMID: 32471464; PMCID: PMC7257174. [PubMed: 32471464]
31. Wang ZB, Liu JY, Xu XJ, Mao XY, Zhang W, Zhou HH, Liu ZQ. Neurodegeneration with brain iron accumulation: Insights into the mitochondria dysregulation. Biomed Pharmacother. 2019; 118:109068. Epub 2019/08/14. doi: 10.1016/j.biopha.2019.109068. PubMed PMID: 31404774. [PubMed: 31404774]
32. Wang W, Wang X, Fujioka H, Hoppel C, Whone AL, Caldwell MA, Cullen PJ, Liu J, Zhu X. Parkinson's disease-associated mutant VPS35 causes mitochondrial dysfunction by recycling DLP1 complexes. Nat Med. 2016;22(1):54–63. Epub 2015/12/01. doi: 10.1038/nm.3983. PubMed PMID: 26618722; PMCID: PMC4826611. [PubMed: 26618722]
33. Wang X, Su B, Lee HG, Li X, Perry G, Smith MA, Zhu X. Impaired balance of mitochondrial fission and fusion in Alzheimer's disease. J Neurosci. 2009;29(28):9090–103. Epub 2009/07/17. doi: 10.1523/jneurosci.1357-09.2009. PubMed PMID: 19605646; PMCID: PMC2735241. [PubMed: 19605646]
34. Jiang S, Nandy P, Wang W, Ma X, Hsia J, Wang C, Wang Z, Niu M, Siedlak SL, Torres S, Fujioka H, Xu Y, Lee HG, Perry G, Liu J, Zhu X. Mfn2 ablation causes an oxidative stress response and eventual neuronal death in the hippocampus and cortex. Mol Neurodegener. 2018;13(1):5. Epub 2018/02/03. doi: 10.1186/s13024-018-0238-8. PubMed PMID: 29391029; PMCID: PMC5796581 through the Case Western Reserve University IACUC board. CONSENT FOR PUBLICATION: Not applicable. COMPETING INTERESTS: XZ. is a paid consultant of Sierra Research Group LLC. The author declares that he/she has no competing interests PUBLISHER'S NOTE: Springer Nature remains neutral with regard to jurisdictional claims in published maps and institutional affiliations. [PubMed: 29391029]
35. Pham AH, Meng S, Chu QN, Chan DC. Loss of Mfn2 results in progressive, retrograde degeneration of dopaminergic neurons in the nigrostriatal circuit. Hum Mol Genet. 2012;21(22):4817–26. Epub 2012/08/04. doi: 10.1093/hmg/dds311. PubMed PMID: 22859504; PMCID: PMC3607482. [PubMed: 22859504]
36. Han S, Nandy P, Austria Q, Siedlak SL, Torres S, Fujioka H, Wang W, Zhu X. Mfn2 Ablation in the Adult Mouse Hippocampus and Cortex Causes Neuronal Death. Cells. 2020;9(1). Epub 2020/01/18. doi: 10.3390/cells9010116. PubMed PMID: 31947766; PMCID: PMC7017224.
37. Oliveira MC, Yusupov M, Bogaerts A, Cordeiro RM. Lipid Oxidation: Role of Membrane Phase-Separated Domains. J Chem Inf Model. 2021;61(6):2857–68. Epub 2021/06/04. doi: 10.1021/acs.jcim.1c00104. PubMed PMID: 34080860. [PubMed: 34080860]
38. Mori A, Hatano T, Inoshita T, Shiba-Fukushima K, Koinuma T, Meng H, Kubo SI, Spratt S, Cui C, Yamashita C, Miki Y, Yamamoto K, Hirabayashi T, Murakami M, Takahashi Y, Shindou H, Nonaka T, Hasegawa M, Okuzumi A, Imai Y, Hattori N. Parkinson's disease-associated iPLA2-VIA/PLA2G6 regulates neuronal functions and α-synuclein stability through membrane remodeling. Proc Natl Acad Sci U S A. 2019;116(41):20689–99. Epub 2019/09/25. doi: 10.1073/pnas.1902958116. PubMed PMID: 31548400; PMCID: PMC6789907. [PubMed: 31548400]
39. Jiang S, Shao C, Tang F, Wang W, Zhu X. Dynamin-like protein 1 cleavage by calpain in Alzheimer's disease. Aging Cell. 2019;18(3):e12912. Epub 2019/02/16. doi: 10.1111/acel.12912. PubMed PMID: 30767411; PMCID: PMC6516178. [PubMed: 30767411]

40. Gao M, Yi J, Zhu J, Minikes AM, Monian P, Thompson CB, Jiang X. Role of Mitochondria in Ferroptosis. Mol Cell. 2019;73(2):354–63.e3. Epub 2018/12/26. doi: 10.1016/j.molcel.2018.10.042. PubMed PMID: 30581146; PMCID: PMC6338496. [PubMed: 30581146]

41. Mao C, Liu X, Zhang Y, Lei G, Yan Y, Lee H, Koppula P, Wu S, Zhuang L, Fang B, Poyurovsky MV, Olszewski K, Gan B. DHODH-mediated ferroptosis defence is a targetable vulnerability in cancer. Nature. 2021;593(7860):586–90. Epub 2021/05/14. doi: 10.1038/s41586-021-03539-7. PubMed PMID: 33981038. [PubMed: 33981038]

Highlights

- MPAN cell models show mitochondrial deficits, iron overload and increased lipid peroxidation.
- Antioxidant NAC and iron chelator DFO restore oxidative damage and mitochondrial dysfunction in MPAN cell models.
- Erastin and RSL3 cause greater ferroptosis in MPAN cell models which could be inhibited by iron chelator DFO pretreatment.
- Biopsied cortical brain tissues from MPAN patient demonstrated mitochondrial deficits and ferroptosis related oxidative damage.

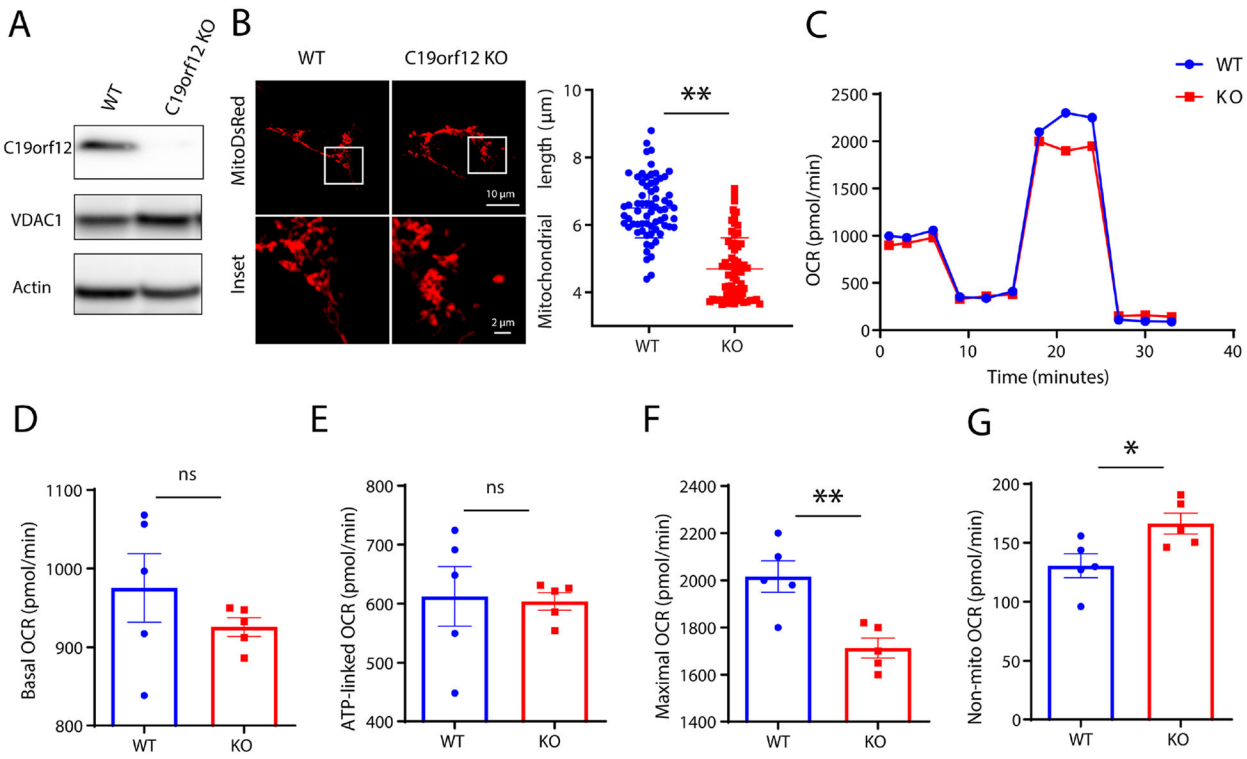

Figure 1. Loss of C19orf12 damaged mitochondria in M17 cells.

(A) Western blot analysis of protein expression of C19orf12 in M17 wildtype (WT) and knockout (KO) cells (n = 3 replicates). (B) Representative confocal images of mitochondria visualized by transfected mito-DsRed and quantification of mitochondrial length on the right (n = 70 cells). (C-G) Representative mitochondria respiration assay in M17 cells (C), quantification of basal oxygen consumption rate (OCR) (D), ATP-linked OCR (E), maximal OCR (F) and non-mito OCR (G) (n = 5 replicates). Results are representative data (Means ± SE) of three independent experiments. Student's t test, * $P < 0.05$, ** $P < 0.01$.

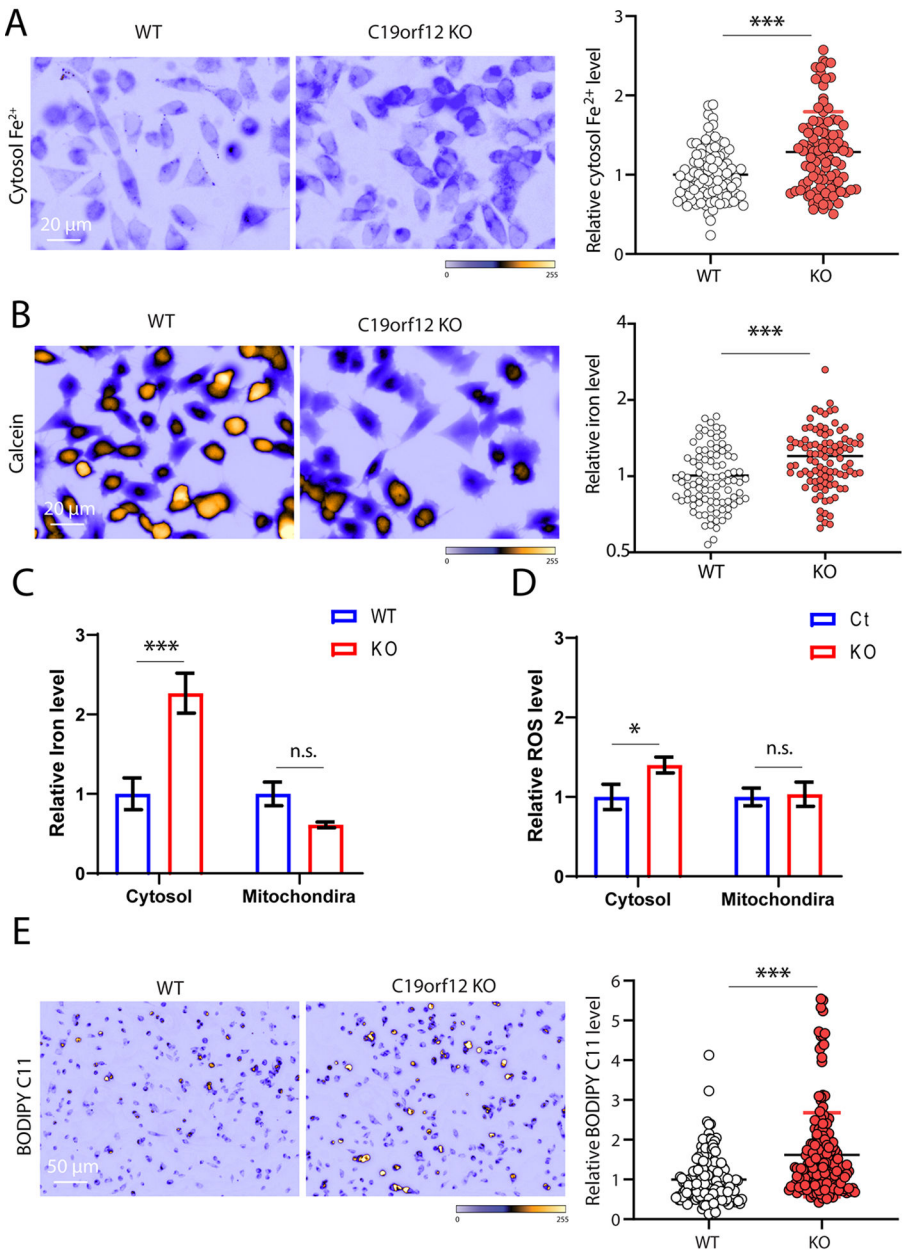

Figure 2. Increased iron levels in C19orf12 KO M17 cells.

(A) Ferric iron was stained by BioTracker Red Fe^{2+} Dye in C19orf12 KO and WT cells (n = 200 cells). (B) Ferrous iron was stained by Calcein AM green in C19orf12 KO and WT cells (n = 100 cells). (C) Iron levels in cytosolic and mitochondrial fraction of C19orf12 KO and WT cells by atom furnace spectrometry (n = 3 replicates). (D) Cytosol ROS levels and mitochondrial ROS levels were analyzed by H2DCFDA and mitoSOX (n = 3 replicates). (E) Lipid ROS levels were analyzed by BODIPY C11 (n = 180 cells). Results are representative data (Means ± SE) of three independent experiments. Student's t test, * $P < 0.05$, *** $P < 0.001$, n.s., $P > 0.05$.

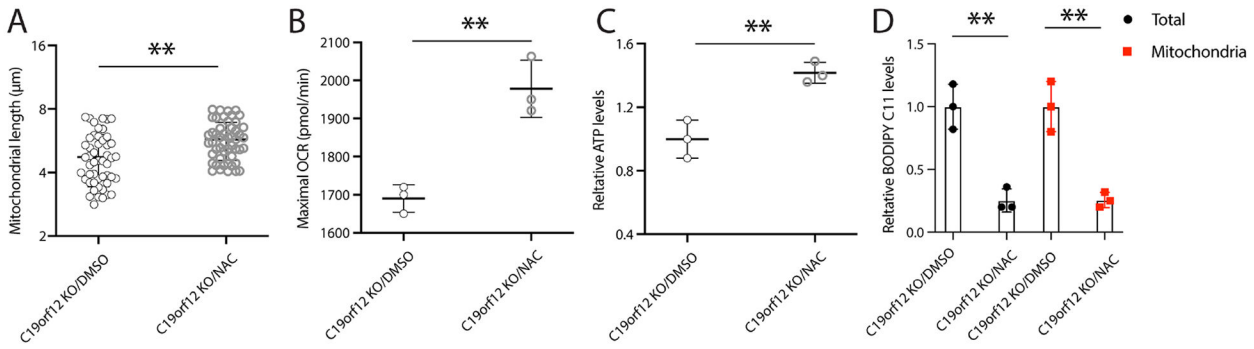

Figure 3. Antioxidant NAC prevented mitochondrial deficits and lipid peroxidation in C19orf12 KO cells.

C19orf12 KO M17 cells were treated by antioxidant NAC (50 mM) for 24 hours: (A) mitochondrial length was analyzed in mito-DsRed transfected cells by confocal images; (B) Mitochondrial respiration assay was performed to analyze maximal OCR; (C) Cellular ATP levels were measured; (D) cytosolic lipid ROS were measured by BODIPY C11 probes. Results are representative data (Means ± SE) of three independent experiments. One-way ANOVA followed by Tukey correction, ** $P < 0.01$, n.s., $P > 0.05$

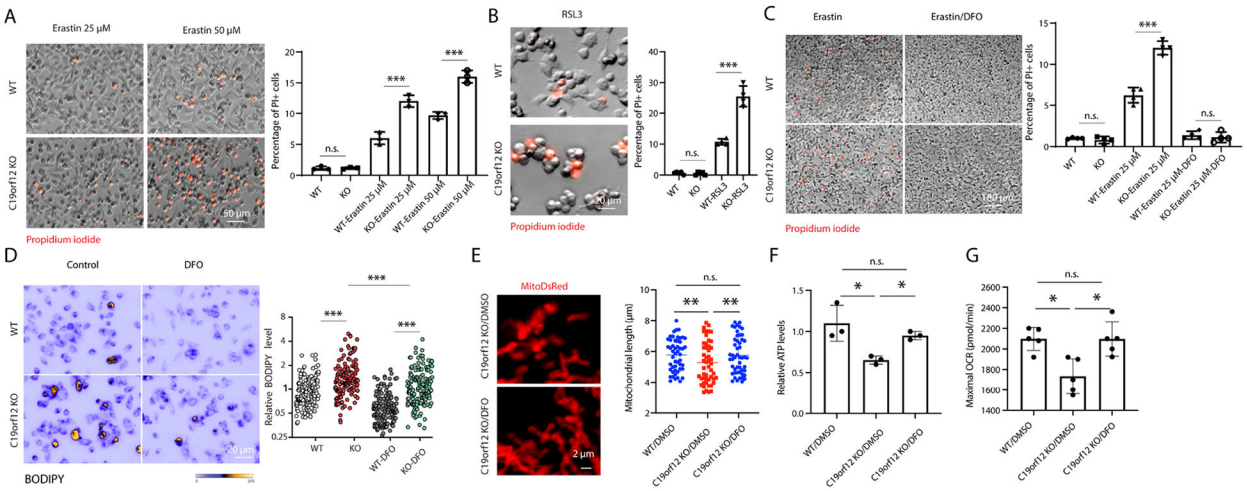

Figure 4. C19orf12 KO cells were associated with ferroptosis.

(A-B) M17 cells were stained by PI after treatment by erastin (25 μM, 50 μM) (A) and RSL3 (10 μM) (B) for 24 hours (n = 3 replicates). (C) Iron chelator DFO treatment (50 μM) rescued cell death in erastin treatment (n = 3 replicates). (D) DFO treatment rescued oxidized lipid in C19orf12 KO cells (n = 150 cells). (E) Mitochondrial fragmentation in C19orf12 KO cells was rescued by DFO treatment (n = 50 cells). (F-G), ATP levels (n = 3 replicates) and maximal OCR (n = 5 replicates) in C19orf12 KO cells were restored after DFO treatment. Results are representative data (Means ± SE) of three independent experiments. One-way ANOVA followed by Tukey correction, * $P < 0.05$, *** $P < 001$, n.s., $P > 0.05$

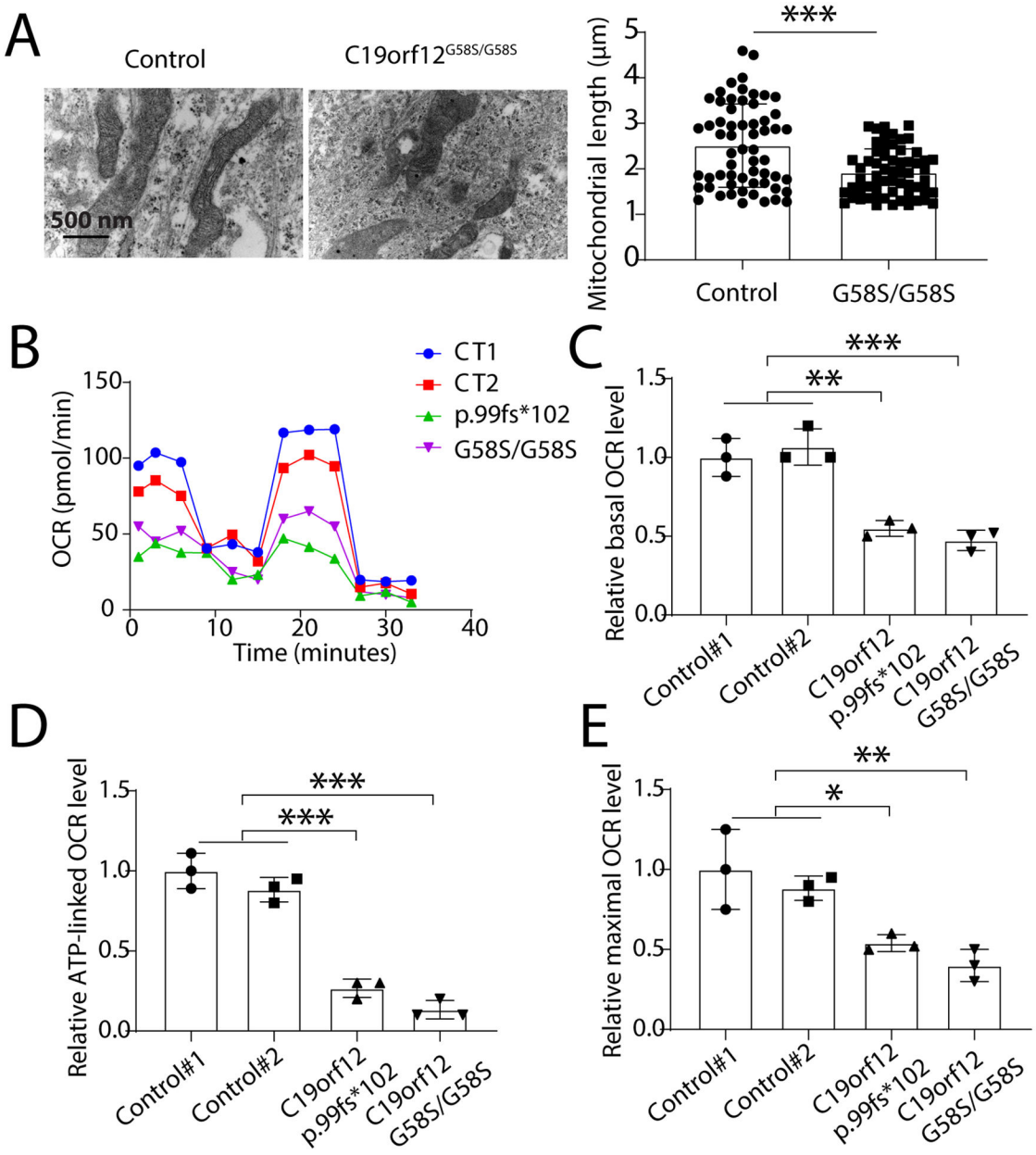

Figure 5. Abnormal mitochondrial function in MPAN skin fibroblasts.

(A) Electron microscopy analysis of mitochondria in cultured human MPAN skin fibroblasts (n = 60 mitochondria from 5 neurons). (B-E) Mitochondria respiration assay of cultured human MPAN skin fibroblasts by Seahorse analyzer (B) and quantification of relative basal oxygen consumption rate (OCR) (C), relative maximal OCR (D) and non-mito OCR (E). Results are representative data (Means ± SE) of three independent experiments. Student's t test and one-way ANOVA followed by Tukey correction, * $P < 0.05$, ** $P < 0.01$, *** $P < 0.001$, n.s., $P > 0.05$

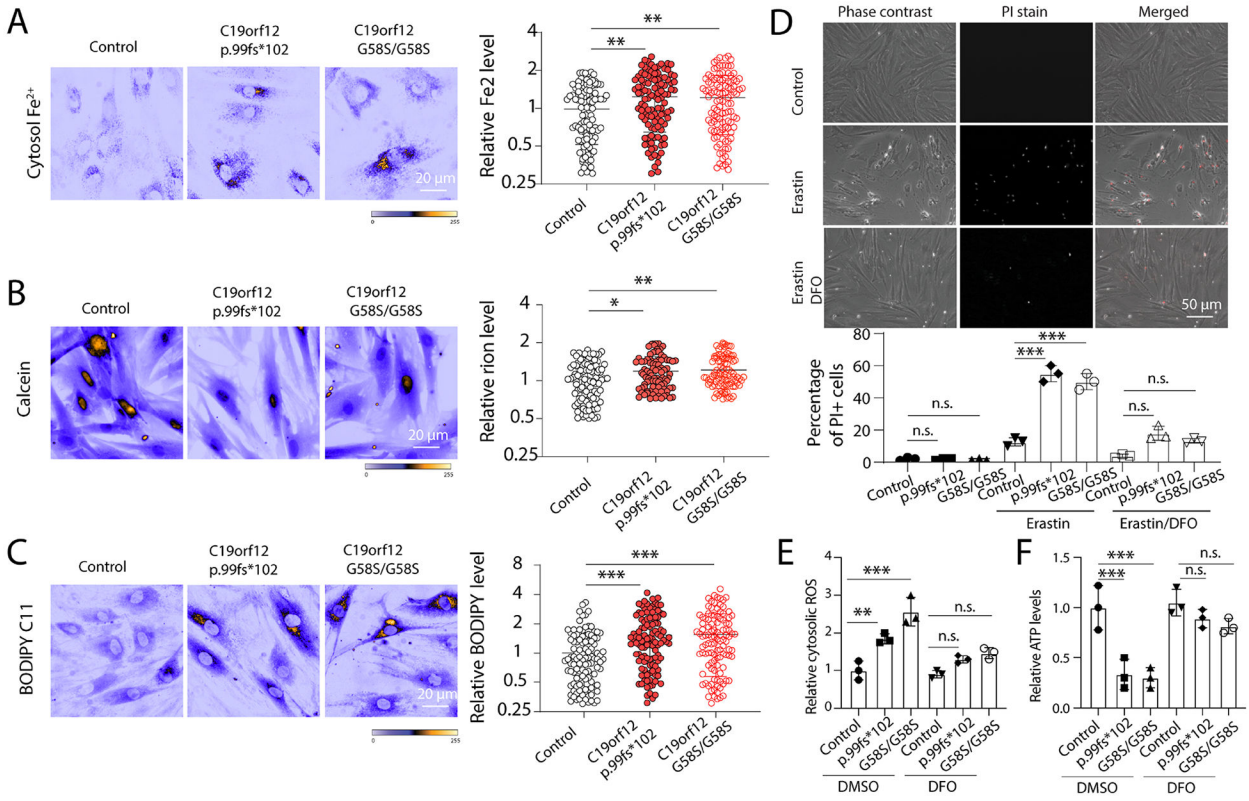

Figure 6. Increased iron levels and ferroptosis in MPAN skin fibroblasts.

(A-B) Iron levels were analyzed by cytosolic ferrous probes (A) and Calcein AM (B) in live culture of MPAN skin fibroblasts with C19orf12$^{G58S/G58S}$ or C19orf12^{p99fs*102} mutations (n = 110 cells). (C) Oxidized lipid levels were analyzed by BODIPY C11 in MPAN skin fibroblasts (n = 110 cells). (D) DFO treatment (50 μM) rescued the cell death caused by erastin in MPAN skin fibroblasts (n = 3 replicates). (E-F) DFO treatment rescued cytosolic ROS levels (E) and ATP levels (F) in MPAN skin fibroblasts (n = 3 replicates). Results are representative data (Means ± SE) of three independent experiments. One-way ANOVA followed by Tukey correction, * P < 0.05, ** P <01. *** p < 0.001, n.s., P > 0.05

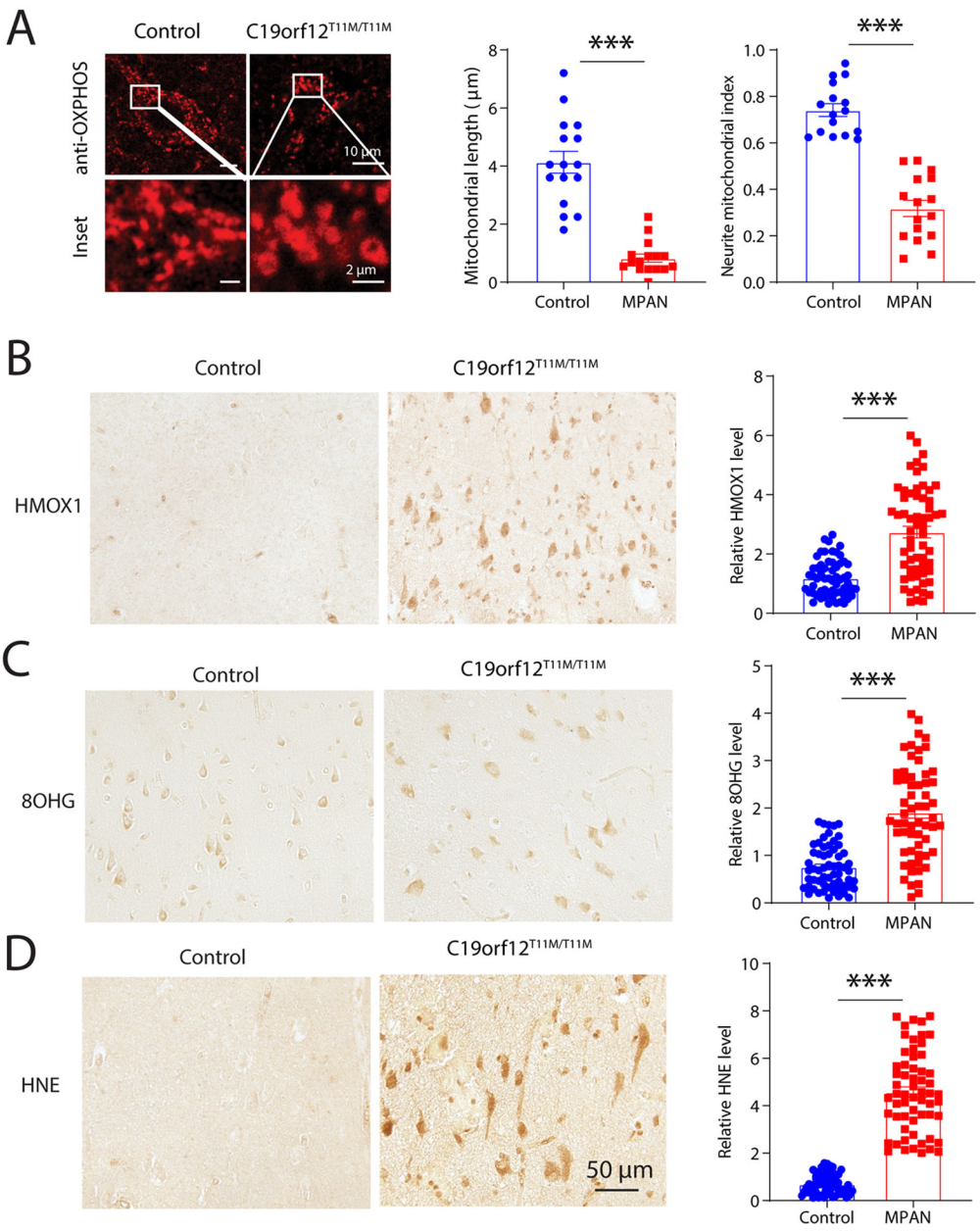

Figure 7. Abnormal mitochondria and ferroptosis related oxidative damages in cortical neurons of MPAN brain.

(A) Representative confocal images of mitochondrial after immunostaining with anti-OXPHOS cocktail antibodies in pyramidal neurons in C19orf12^{T11M} MPAN cortical tissues. Right, quantification of mitochondrial length and neurite mitochondrial index in neurons (n = 16 neurons). (B-D) Representative immunohistochemistry images of staining with anti-HMOX1 antibodies (B), anti-8OHG antibodies (C) and anti-HNE antibodies (D) in C19orf12^{T11M} MPAN cortex sections (n = 60 cells). Results are representative data (Means ± SE) of three independent experiments (n = 3 replicates). Student's t test, *** P < 0.001.